IMPACT OF COMPUTING IN SCIENCE AND ENGINEERING 3, 305–329 (1991)

Symmetry Breaking and the Interaction of Hyperbolic Waves

MOHSEN MAESUMI

Department of Mathematics, Lamar University, Beaumont, Texas 77710

Received July 30, 1990

M. Maesumi, Symmetry Breaking and the Interaction of Hyperbolic Waves, *IMPACT of Computing in Science and Engineering* **3**, 305–329 (1991).

Hyperbolic conservation laws have scale invariance symmetry. In this paper we study an example of the breaking of such symmetry which occurs when the coefficients of a scalar hyperbolic equation are themselves solutions of an elliptic equation. Our model problem is related to wave refraction that occurs during two-phase incompressible flow in a porous medium consisting of two homogeneous layers. With the aid of formal and computational mathematics we study the evolution of the angles made by intersecting discontinuities. The space of scale symmetric solutions for the refraction problem changes discontinuously at a certain point in the parameter space. At this point the solution space is two-dimensional, but at other points it is one- or zero-dimensional, i.e., isolated. We introduce approximate scale breaking elementary waves as formal constructions which give a uniform two-dimensional solution space. A stability analysis determines the region of the parameter space where the isolated exact solutions are stable. Our numerical experiments give an independent verification of the formal results.

1. INTRODUCTION

Recent years have seen remarkable progress in the understanding of scale symmetric solutions for hyperbolic conservation laws [1–5]. These solutions are known as Riemann solutions; the Cauchy problem they solve is the Riemann problem, i.e., the initial value problem for a hyperbolic conservation law with data invariant under $(\mathbf{x}, t) \to (\alpha\mathbf{x}, \alpha t)$ for $\alpha > 0$. Striking new phenomena in the form of novel nonlinear wave structures and wave interactions have been discovered and shown to arise in important examples.

Symmetry breaking occurs when the solution of a differential equation has a smaller symmetry group than that of the equation and its data. Although translational symmetry breaking for Riemann solutions has been considered previously [6–9], scale symmetry breaking has received less consideration. The central point of this paper is that scale invariance symmetry breaking

0899-8248/91 $3.00

has a role to play in the analysis of hyperbolic wave interactions. We consider a class of hyperbolic conservation laws and a point in the parameter space of these equations at which the space of symmetric solutions changes discontinuously. In a neighborhood of such a point there can be no uniformly valid asymptotics within the class of symmetric solutions.

In this paper we study approximate scale breaking solutions of Riemann problems. The equations are a simplified version of those for two-phase flow in porous media in two spatial dimensions, as motivated by petroleum engineering. The Riemann problem we consider is the interaction of a phase discontinuity in the fluid, i.e., a Buckley–Leverett front, with a geological layer, i.e., a jump discontinuity in the equation coefficients. The point of interaction of the layer interface and the front is called a node. The Riemann solution is largely determined by the dynamically stable angles formed between the front and the layer interface at the node. It can thus be thought of as a wave refraction problem, or a nonlinear extension of Snell's law.

The refraction of a wave front at a medium discontinuity is termed *passive* if the incoming front can have an arbitrary configuration with respect to the interface. For example, the refraction of light by an air–water interface is passive. In contrast, we call a refraction process *active* if the configuration of the incoming front is determined by the process. Glimm and Sharp [10] observed this phenomenon in their analysis of two-phase incompressible flow in a porous medium that is composed of two homogeneous regions of distinct permeability. The incompressibility condition results in an elliptic equation for the pressure which allows the downstream data to influence the upstream velocity field. This velocity, in turn, modifies the configuration of the incoming front until a specific angle of incidence forms.

In our similar model equations, the velocity is proportional to the gradient of the pressure which satisfies an elliptic equation. It is well known that elliptic equations do not have regular solutions at a "corner" in the domain of the equation. This implies that the velocity at the node is not, in general, finite (it can be zero or infinity). Rather the velocity has a power law dependence on the distance from the node. In order to study nonfinite velocities in the refraction we introduce approximate elementary waves. These are singular, scale breaking, transient constructions which satisfy Snell's law on a circle centered at the node. The strength of the singularity in the velocity field at the node determines the relaxation time for these constructions to achieve stable configurations.

2. The Flow Equations

The model equations governing two-phase (e.g., water and oil) incompressible flow in porous media, in the absence of capillary and gravity forces, are

$$\phi(\mathbf{x})s_t + \nabla \cdot f(s, \mathbf{x})\mathbf{v} = 0, \tag{1a}$$

$$\mathbf{v} = -\Lambda(s, \mathbf{x})\nabla P, \tag{1b}$$

$$\nabla \cdot \mathbf{v} = \nabla \cdot \Lambda \nabla P = 0. \tag{1c}$$

Here s is the saturation of the water phase, measured as the volume fraction of the fluid mixture. The total flux, or volumetric velocity, of the fluid mixture is denoted $\mathbf{v}$. The fractional flow function f is defined so that $f\mathbf{v}$ is the volumetric velocity of the water phase. ϕ is the medium porosity, the fraction of the bulk volume available to the flow. Λ is the transmissibility tensor of the flow and P is the fluid pressure.

Nonlinear hyperbolic equations such as (1a) tend to form weak solutions that are discontinuous along curves called shock fronts [11–13]. We consider the propagation of a shock in a medium where Λ is discontinuous across a curve which we call a layer interface. Such an interface marks the boundary between geologically distinct regions or layers in a medium. Typically ϕ, f, and hence s, are also discontinuous across an interface. We shall assume, however, that ϕ, f, and hence s, are continuous so as to reduce the number of independent parameters in the problem. As a further simplification we assume Λ is a scalar and is given by $\Lambda \equiv \lambda(s, \mathbf{x}) = m(s)k(\mathbf{x})$, where $m(s) > 0$ is the *mobility* of the fluid, and $k(\mathbf{x}) > 0$ is the *permeability* of the medium. We consider an idealized medium where ϕ and f are independent of $\mathbf{x}$, and k is constant in each layer. Thus it follows that our main conclusion, concerning symmetry breaking, is important in the simplest possible case, and is not dependent on fine details of the problem formulation.

The selection of a physically correct discontinuity solution of hyperbolic conservation laws is an important, well-known, problem, for which there are a variety of partial answers. Diffusion terms are often used in this context, but are not a panacea, in that, for certain systems, the preferred solutions depend sensitively on the ratios of the components of the diffusion matrix in the limit of small diffusion [14].

For one-dimensional Buckley–Leverett flow with a discontinuous fractional flow function the Riemann solution develops a standing wave at the discontinuity which may interact with other waves passing through the site. In the case of a double layer discontinuity, the solution behaves discontinuously in the limit as the double layer thickness approaches zero [15]. A similar phenomenon is known from combustion theory, in which a thin double layer temperature discontinuity (i.e., a spark) will initiate combustion and cause a distinct solution.

The thrust of this paper is, however, distinct. Not only do we consider single rather than double layers, but, moreover, our problem has too few, not too many scale symmetric solutions. The scale symmetric solutions we consider are composed of waves which satisfy viscosity entropy conditions. In

this sense, symmetry breaking, rather than the entropy condition (i.e., existence rather than uniqueness), is the subject of this paper.

3. Jump Conditions

At each point on a discontinuity curve C, a pair of jump conditions are satisfied which express the incompressibility of the flow and the continuity of the pressure. Assume $\mathbf{n}$ is a unit vector normal to C at $(\mathbf{x}_0, t)$ and $\mathbf{t}$ is a vector tangent to C at the same point. For any quantity $q(\mathbf{x}, t)$, define q_- and q_+ at $(\mathbf{x}_0, t)$ by

$$q_\pm = \lim_{\epsilon \to 0^\pm} q(\mathbf{x}_0 + \mathbf{n}\epsilon, t). \tag{2}$$

Then, using (1b) and (1c), the jump conditions for the velocity at $\mathbf{x}_0$ can be written as

$$\mathbf{v}_- \cdot \mathbf{n} = \mathbf{v}_+ \cdot \mathbf{n} \equiv \nu_n, \tag{3a}$$

$$\frac{\mathbf{v}_- \cdot \mathbf{t}}{\lambda_-} = \frac{\mathbf{v}_+ \cdot \mathbf{t}}{\lambda_+}. \tag{3b}$$

Assume $\mathbf{n}$ is oriented such that the normal flux $\nu_n > 0$. If C is a shock front then we define the *mobility ratio* as $M = \lambda_-/\lambda_+$. The "primary" shock speed is $\sigma = (f(s_+) - f(s_-)/(s_+ - s_-)$, while the propagation speed of the shock is $\sigma\nu_n/\phi$. If C is a layer interface then we define the *permeability ratio* as $K = \lambda_-/\lambda_+$.

We derive a sharp bound for the strength of the singularity of the velocity field for approximate elementary waves in terms of the frontal mobility ratio M. For $M \approx 1$ the singularity is weak and scale breaking solutions are dominant. For $M \ll 1$ the isolated elementary wave solutions, obtained by Glimm and Sharp, are shown to be stable. Moreover, stability improves if the upstream layer is more permeable than the downstream layer, i.e., $K > 1$. Our results are incomplete for $M \gg 1$. It appears that the only stable solutions in the latter case occur when the incoming front, the velocity field, and the layer are tangential at the node. Numerical experiments also indicate that when $M \gg 1$ the layer-shock node acts as a nucleation site for a fluid fingering instability.

4. Elementary Waves

Elementary waves are the simplest discontinuous solutions of nonlinear hyperbolic equations. We define an elementary wave $E(\mathbf{x}, t) = (s(\mathbf{x}, t), \mathbf{v}(\mathbf{x},$

$t)$), wherever s and $\mathbf{v}$ are well defined, as a scale invariant traveling wave solution of (1). Thus

$$E(\alpha\mathbf{x}, \alpha t) = E(\mathbf{x}, t) \qquad \text{for all} \qquad \alpha > 0, \tag{4a}$$

$$E(\mathbf{x} + \mathbf{U}T, t + T) = E(\mathbf{x}, t) \qquad \text{for all } T, \tag{4b}$$

where $\mathbf{U}$ is the propagation velocity of the wave. See also [16–19]. Here we assume that ϕ, f, and Λ satisfy (4), i.e., they are independent of $\mathbf{x}$ except possibly for a discontinuity along a line parallel to $\mathbf{U}$. We give a partial characterization of elementary waves in the following lemma.

LEMMA 1. *Let* $\mathbf{N}_t = \mathbf{U}t$ *denote the location of the node at time* t. *Denote a normal to* $\mathbf{x} - \mathbf{N}_t$ *by* $\mathbf{n}$. *If* E *is an elementary wave solution of* (1) *then at any time* t, E *is constant on rays in the* $\mathbf{x}$ *plane that start at* $\mathbf{N}_t$ *and on which* E *is well defined. If* $\mathbf{v}$ *is smooth in a region* Ω *then* $\mathbf{v}$ *is constant in* Ω. *If* $\mathbf{v} = \mathbf{v}_1$ *in* Ω_1, $\mathbf{v} = \mathbf{v}_2$ *in* Ω_2, $\mathbf{v}_1 \neq \mathbf{v}_2$, *and a smooth curve* C *in the common boundary of* Ω_1 *and* Ω_2 *then* C *is a straight line. If* s *varies smoothly across a ray from* $\mathbf{N}_t$ *that passes through* $\mathbf{x}$ *then* $f'(s)\mathbf{v}\cdot\mathbf{n} = \phi\mathbf{U}\cdot\mathbf{n}$. *If* s *has a jump across the ray then* $\sigma\mathbf{v}\cdot\mathbf{n} = \phi\mathbf{U}\cdot\mathbf{n}$.

Proof. From (4) we have for all $\alpha > 0$

$E(\mathbf{x}, t) = E(\mathbf{x} - \mathbf{U}t, 0) = E(\alpha(\mathbf{x} - \mathbf{U}t), 0) = E(\alpha(\mathbf{x} - \mathbf{U}t) + \mathbf{U}t, t) = E(\alpha(\mathbf{x} - \mathbf{N}_t) + \mathbf{N}_t, t)$. Therefore E is constant on rays that start at $\mathbf{N}_t$. If $\mathbf{v}$ is smooth in Ω then its divergence is zero. From above, $\mathbf{v}$ is constant on rays starting at the node, hence it should be also constant in the direction normal

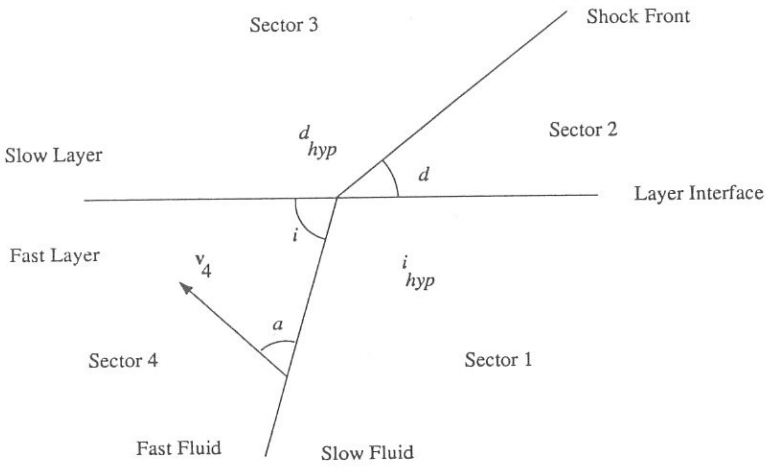

FIG. 1. The notation for the layer-shock interaction. Sector 4, by definition, has the maximum transmissibility, $i = \alpha_4$. In this picture $i_{\text{hyp}} = \alpha_1$.

to these rays. Therefore $\mathbf{v}$ is constant in Ω. If $\mathbf{v}_1$ and $\mathbf{v}_2$ are separated by C and $\tilde{\mathbf{n}}$ is the unit normal to C then by continuity of the normal velocity $\tilde{\mathbf{n}} \cdot (\mathbf{v}_1 - \mathbf{v}_2) = 0$. Since $\mathbf{v}_1 - \mathbf{v}_2$ is a constant nonzero vector then $\tilde{\mathbf{n}}$ should be constant along C. Therefore C is a straight line. Finally define $\zeta = \mathbf{x} - \mathbf{U}t$. Where s is smooth, (1a) can be written as $(-\phi\mathbf{U} + f'(s)\mathbf{v}) \cdot \nabla_\zeta s = 0$. Since s is not constant and $\mathbf{n}$ is perpendicular to ζ we have $(-\phi\mathbf{U} + f'(s)\mathbf{v}) \cdot \mathbf{n} = 0$. If s has a jump across the ray then a similar argument based on the integral form of (1a) gives $(-\phi\mathbf{U} + \sigma\mathbf{v}) \cdot \mathbf{n} = 0$, yielding the required results.

In an elementary wave the region where s varies smoothly is called a fan. In our problem we assume that a single shock divides the plane into two regions with the saturation being constant on either side of the shock (i.e., no fan is present). The wave refraction problem is an example of a co-dimension 2 elementary wave. In Proposition 1, below, we identify all elementary waves for our model problem.

5. The Layer-Shock Interaction

Consider a layer-shock interaction as depicted in Fig. 1. In sector j ($j = 1, 2, 3, 4$) the transmissibility is λ_j, the velocity is $\mathbf{v}_j$, and the opening angle of the sector is α_j. The angle between $\mathbf{v}_4$ and the front is denoted a.

The elliptic and the hyperbolic equations differentiate amongst the four sectors, the former according to the magnitude of the transmissibility and the latter according to the flow direction. To reflect this fact we define two "angles of incidence"; i for the elliptic equation, and i_{hyp} for the hyperbolic equation. Here i is the opening angle of the sector with the maximum transmissibility

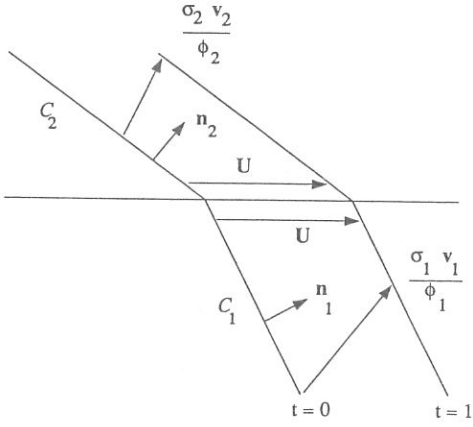

FIG. 2. Dynamical consistency condition. Both components of the wave propagate with the same velocity.

and i_{hyp} is the opening angle of the sector that is upstream with respect to both the shock front and the layer interface. The "angles of refraction," d and d_{hyp}, are then defined as the opening angles of the sectors opposite to i and i_{hyp}, respectively. Hence d is the opening angle of the sector with the minimum transmissibility and d_{hyp} is the opening angle of the sector which is downstream with respect to both the front and the interface.

We shall assume that Sectors 1 and 4 (respectively, 2 and 3) constitute the fast layer (respectively, the slow layer). Similarly Sectors 3 and 4 (respectively, 1 and 2) constitute the fast phase (respectively, the slow phase). Therefore Sector 4 has the maximum transmissibility. We define the transmissibility ratios $R_m = \lambda_4/\lambda_1 = \lambda_3/\lambda_2$ and $R_k = \lambda_1/\lambda_2 = \lambda_4/\lambda_3$. Hence $R_m \geqslant 1$, $R_k \geqslant 1$, $i = \alpha_4 = \pi - \alpha_1$, and $d = \alpha_2 = \pi - \alpha_3$. R_m and R_k, unlike M and K, are independent of the flow direction.

The distinction between i and i_{hyp} becomes important only when we discuss stability. i is identified with Sector 4 but i_{hyp} can be any of the four sectors. In the last part of Proposition 1 we will see that there is an isolated elementary wave for each of these four possibilities. (See Fig. 5 below.)

5.1. *Dynamical Consistency Condition for Layer-Shock Interactions*

Assume that C_1 and C_2 are the two segments of a shock front in an elementary wave solution of a layer-shock interaction that is propagating with velocity $\mathbf{U}$ along the layer interface. (See Fig. 2) Let $\mathbf{n}_j$, $j = 1, 2$, represent a normal to C_j, $\mathbf{v}_j \cdot \mathbf{n}_j$ the volumetric velocity in the direction normal to C_j, ϕ_j the porosity, and σ_j the primary shock speed for C_j. Then from Lemma 1 we have

$$\sigma_1 \mathbf{v}_1 \cdot \mathbf{n}_1 = \phi_1 \mathbf{U} \cdot \mathbf{n}_1, \qquad \sigma_2 \mathbf{v}_2 \cdot \mathbf{n}_2 = \phi_2 \mathbf{U} \cdot \mathbf{n}_2. \tag{5}$$

The assumption of continuity of f and ϕ across the layer implies $\sigma_1 = \sigma_2$ and $\phi_1 = \phi_2$. Using these facts we write the law of refraction for elementary wave solution as

$$\frac{\mathbf{v}_1 \cdot \mathbf{n}_1}{\mathbf{U} \cdot \mathbf{n}_1} = \frac{\mathbf{v}_2 \cdot \mathbf{n}_2}{\mathbf{U} \cdot \mathbf{n}_2}. \tag{6}$$

We call this the *dynamical consistency condition.* (The *local* propagation velocity $\mathbf{v}$ is consistent with the *global* propagation velocity $\mathbf{U}$.)

5.2. *Elementary Waves for Layer-Shock Interactions*

The layer-shock elementary waves are specified by two transmissibility ratios, R_m and R_k, and three angles, a, i, and d. One might expect that once R_m, R_k, i, and a are given then d can be determined. This is, however, im-

possible in most cases. There are "very few" elementary wave solutions of (1). In fact if we specify R_m, R_k, i, and a then the system of equations that relates velocities and angles through the jump conditions and the dynamical consistency condition will be overdetermined.

PROPOSITION 1. *The only possible configurations for an elementary wave of the type in Fig.* 1 *are:*

(I) *A plane wave solution for* $R_k = 1$. *Here a and* R_m *are arbitrary and* $d = i$. *This is a trivial solution in which the two layers are identical and there is no refraction.*

(II) *A family of passive refraction solutions for* $R_m = 1$. *Here* R_k, *i, and a are arbitrary and the angle of refraction is given by*

$$\cot d = \cot i - \left(1 - \frac{1}{R_k}\right)\cot(i + a). \tag{7}$$

(*See Fig.* 3.) *These solutions are also important in the verification of numerical procedures.*

(III) *A family of stationary wave solutions. In this case* $a = 0°$ *or* $180°$, *i.e., the flow is parallel to the front. Here i,* R_k, *and* R_m *are arbitrary and the angle of refraction is given by*

$$\tan d = R_k \tan i. \tag{8}$$

(*See Fig.* 4.) The node velocity for these solutions is $\mathbf{U} = 0$.

(IV) *Four isolated solutions. In this case* $a = 90°$, *i.e., the flow is normal*

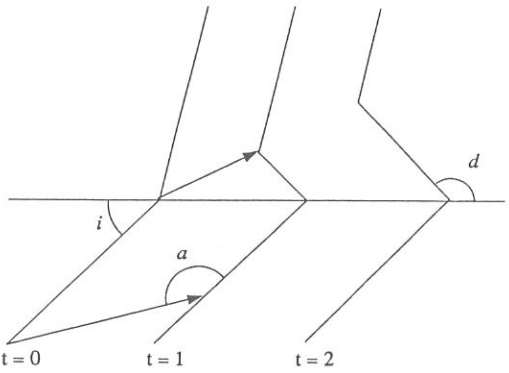

FIG. 3. The solution of a Riemann problem for unit mobility ratio. Note that the steady angles on the refracted side are not present in the initial data but are established dynamically.

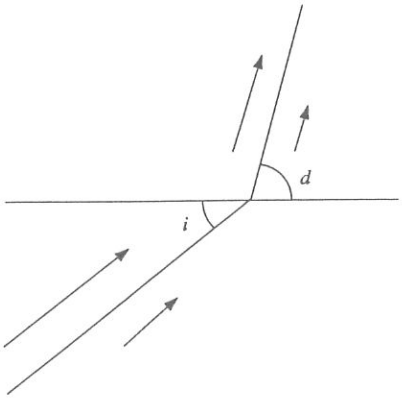

FIG. 4. A stationary elementary wave.

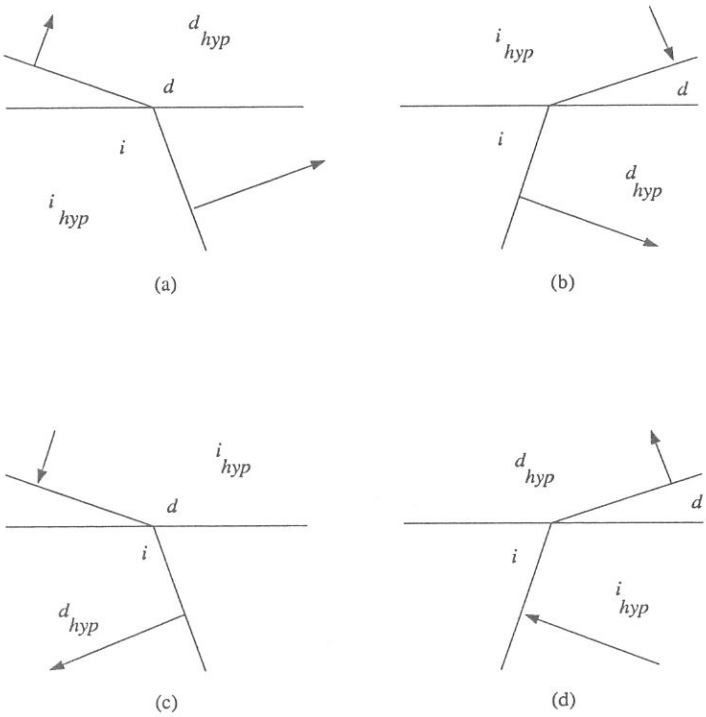

FIG. 5. The isolated elementary waves. The angles of incidence and refraction are only a function of the permeability ratio.

to the front. (See Fig. 5.) Here R_m and R_k are arbitrary but both i and d are determined in terms of R_k:

$$\tan i = \pm\sqrt{R_k}, \qquad \tan d = \pm 1/\sqrt{R_k}. \tag{9}$$

Hence, in terms of the number of angular degrees of freedom, type II solutions are two-dimensional, type III solutions are one-dimensional, and type IV solutions are zero-dimensional. For a proof of Proposition 1 see [10].

In Proposition 2, below, we express the fact that when the incoming front makes a small angle with the layer, then the front will pass through the interface without significant refraction, provided that the velocity field does not also make a small angle with the front.

PROPOSITION 2. *In a configuration where $i = d$ the jump conditions and Snell's law can be satisfied up to a relative error of $O(\sin i/\sin a)$.*

Here we sketch the proof of this proposition; for further details see [20]. We start with a velocity $\mathbf{v}_4$ in Sector 4 and given values for i and d. To compute the velocity in Sector 2 we can either use the jump conditions across the 4–1 and 1–2 sectors to obtain $\mathbf{v}_2$ or use the jump conditions across the 4–3 and 3–2 sectors to obtain $\mathbf{v}_2'$. In general $\mathbf{v}_2 \neq \mathbf{v}_2'$. We notice that when $\sin a \neq 0$ the propagation velocity of the node tends to infinity as $\sin i \to 0$. The difference between the node propagation velocity as defined by the incident side and the refracted side will be finite if and only if $i = d$. When $i = d$ the relative error in the node propagation velocity will be $O(\sin i/\sin a)$. The discrepancy between $\mathbf{v}_2$ and $\mathbf{v}_2'$ may be measured by $\|\mathbf{v}_2 - \mathbf{v}_2'\| / \|\mathbf{v}_4\|$, and is $O(\sin i)$.

6. APPROXIMATE ELEMENTARY WAVES

We have shown that the space of layer-shock elementary wave solutions of (1) is disconnected. In particular, the structure of the solution space changes at $R_m = 1$. This prompts us to search for approximate solutions in order to obtain a uniform description of layer-shock interactions and their evolution. In this section we present a class of approximate solutions which have the correct limiting behavior near all the exact solutions. These constructions, at a given time, satisfy the elliptic equation (1c) exactly, but (1a), (4), and (6) are only approximately satisfied. Our analysis of the approximate elementary waves is at the level of formal mathematics and numerical analysis.

To introduce the approximate elementary waves, we start by assuming that the wave has a configuration similar to Fig. 1 with the shock front approximated by straight lines near the node. We note that the general solution of the pressure equation (1c), subject to the jump conditions, has an elliptic singularity at the node. Thus the pressure has a power law dependence on the distance from the node, of the form r^l, and the power l is near 1. As a

result the velocity is proportional to r^{l-1}, which is either zero or infinity at the node. To avoid the singularity we shift the focus of calculations from the node to the perimeter of a circle centered at the node. This circle is denoted as the base circle and we indicate its radius by r_0.

The justification for the introduction of a new length scale r_0 into our calculations lies in the fact that the idealized physical model (1) ignores the capillary length scale H_{cap}. In order to compare to our numerical calculations, which employ a discretization length scale $H_{\text{dis}} > H_{\text{cap}}$, we use a length scale $r_0 \approx H_{\text{dis}}$ in our theoretical derivations. It should be emphasized that the numerical value of r_0 does not explicitly enter the computations; instead we use dimensionless quantities (such as angles and velocity ratios) measured on the base circle.

We return to the solution of the pressure equation (1c). In a region where λ is constant the pressure is a harmonic function $\Delta P = 0$. Since the plane is divided into four sectors bounded by straight lines we can use separation of variables in polar coordinates to solve $\Delta P = 0$ in each sector. Then the separation constant l^2 and the coefficients of the eigenfunction expansion for each sector are determined by satisfying the jump conditions.

When the mobility ratio is $M = 1$ the solution of the pressure equation can be written in terms of a linear combination of real and imaginary parts of z^n, $n = 0, \pm 1, \pm 2, \ldots, z = x + y\sqrt{-1}$. (Since there is no source, sink, or multipole at the node we disregard the negative and zero eigenvalues.) For each eigenvalue n there are two independent eigenfunctions. For example, the leading pair of eigenfunctions corresponding to $n = 1$ are $x \equiv r \cos\theta$ and $y \equiv r \sin\theta$.

To satisfy the jump conditions across both the layer and the front when $M \neq 1$ the eigenfunctions have to be a linear combination of real and imaginary parts of z^l, where in general l is not an integer. Moreover the degeneracy of the eigenvalues is removed and in general there is only one eigenfunction for each eigenvalue. In this case we write the nonnegative eigenvalues as $0 < l_1 \leq \tilde{l}_1 < l_2 \leq \tilde{l}_2 \cdots$.

To obtain the eigenvalues and the eigenfunctions we set up a system of linear homogeneous equations which expresses the jump conditions across the discontinuity lines. To obtain a nontrivial solution we set the determinant of the system equal to zero yielding an equation for the exponent l

$$4\sin^2(l\pi) + \prod_{1\leq k\leq 4} \cos(l\alpha_k) \sum_{1\leq i<j\leq 4} \frac{(\lambda_i - \lambda_j)^2}{\lambda_i\lambda_j} \tan(l\alpha_i)\tan(l\alpha_j) = 0. \quad (10)$$

The solution l of this equation is a function of the angles and the transmissibility ratios which we may express as $l = l(i, d, R_m, R_k)$.

Once the values of l are determined then the eigenfunction expansion for the pressure can be written. To perform a leading order analysis (in r) we

focus on the $(l_1, \tilde{l}_1)$ pair. These are the first two positive solutions of (10). (We emphasize that using l_1 alone to represent the flow near the node is incorrect since the eigenfunctions corresponding to l_1 and $\tilde{l}_1$ are both approximately linear and are of comparable numerical magnitude. Moreover if l_1 is the dominant mode then our formalism automatically accounts for that.)

Let $\mathbf{V}_1$ and $\tilde{\mathbf{V}}_1$ represent the leading pair of velocity eigenfunctions corresponding to $(l_1, \tilde{l}_1)$. Then to leading order the velocity $\mathbf{V}$ can be written $\mathbf{V} = \beta\mathbf{V}_1 + \tilde{\beta}\tilde{\mathbf{V}}_1$. Let I and D be the points of intersection of the base circle with the front. (See Fig. 6.) Then we call $(i, d, \beta, \tilde{\beta}, r_0)$ an *approximate elementary wave* if

$$\frac{\mathbf{V}_I \cdot \mathbf{n}_I}{\mathbf{U} \cdot \mathbf{n}_I} = \frac{\mathbf{V}_D \cdot \mathbf{n}_D}{\mathbf{U} \cdot \mathbf{n}_D}. \tag{11}$$

Here $\mathbf{n}_I$ and $\mathbf{V}_I$ (respectively $\mathbf{n}_D$ and $\mathbf{V}_D$) are the unit normal vector to the front and the velocity $\mathbf{V}$ at I (respectively D), and $\mathbf{U}$ is parallel to the layer interface.

When i and d are given, (11) is a linear homogeneous equation in β and $\tilde{\beta}$, and has a unique solution (up to a multiplicative constant). However, if $\mathbf{V}_I$ and i are given, (11) may fail to have a solution or the solution may fail to be unique. The nonuniqueness can be seen even in the exact solutions when $M = 1$. In this case if the flow is parallel to the interface then for any i both $d = 0$ and $d = \pi$ are solutions of (7). For $M \neq 1$, nonuniqueness or nonexistence occurs when the flow is approximately parallel to the layer interface.

To specify an approximate elementary wave we indicate two of the three angles (i, d, a). Here a is the angle between the velocity field $\mathbf{V}$ in Sector 4 and the front at the point I. (See Fig. 6.) Figure 7 shows contours of a as a

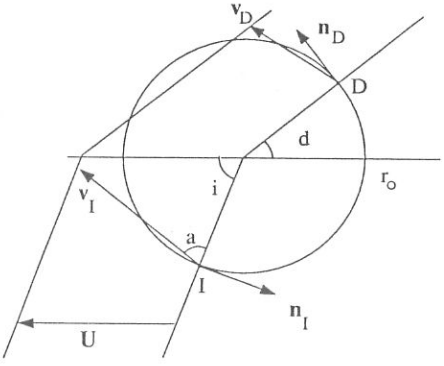

FIG. 6. The calculations for approximate elementary waves are performed on the base circle.

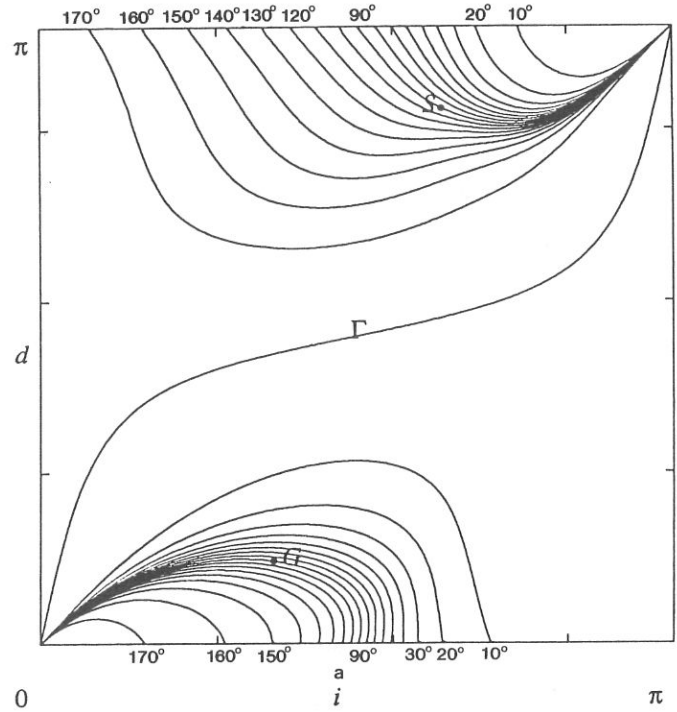

FIG. 7. The angle of refraction d vs the angle of incidence i for selected values of the angle between the flow and the front a. Each curve corresponds to a specific value of a which is denoted in degrees on the horizontal edges of the plot. The points G and S and the curve Γ correspond to the solutions obtained by Glimm and Sharp. Here $R_m = 10$ and $R_k = 5$.

function of i and d for $R_m = 10$ and $R_k = 5$. Points G and S correspond to the solutions of (9) and the curve Γ corresponds to the solutions of (8). All contours, except Γ, are tangential to the $i = d$ line at $(0, 0)$ and (π, π). The solutions on these contours in the vicinity of $(0, 0)$ and (π, π) are comparable to the solutions suggested by Proposition 2.

6.1. *The Strength of the Singularity*

The strength of the singularity at the node depends on the deviation of l_1 and $\tilde{l}_1$ from unity. For given angles i and d these deviations depend on R_m and R_k but the maximum deviation depends only on R_m. One can use (10) to show

$$\max_{0\leq i,d\leq\pi} (1 - l_1) = \max_{0\leq i,d\leq\pi} (\tilde{l}_1 - 1) = \frac{1}{\pi} \sin^{-1} \frac{R_m - 1}{R_m + 1}. \qquad (12a)$$

Table I shows extreme values of l_1 and $\tilde{l}_1$ for selected values of the mobility ratio. The radial dependence of the first velocity eigenfunction is through $g(r) = r^{l_1-1}$. This velocity may tend to infinity as r approaches zero. In that case g will double if r is reduced by a factor of $\gamma = 2^{1/(1-l_1)}$. The approximate minimum value of γ is indicated in Table I.

As a general rule the singularity is very weak and it is necessary to use very large or very small values of M to get an appreciable singularity. One can also use (10) to show

$$\max_{0\leqslant i=d\leqslant\pi} (1 - l_1) = \max_{0\leqslant i=d\leqslant\pi} (\tilde{l}_1 - 1) = \frac{1}{\pi} \sin^{-1} \frac{(R_m - 1)(R_k - 1)}{(R_m + 1)(R_k + 1)}. \quad (12b)$$

We see that the influence of the layer interface on the singularity strength decreases as R_k approaches unity.

6.2. *The Stability and Evolution of Approximate Elementary Waves*

In this section we give an intuitive description of the evolution of approximate elementary waves. Ideally one needs a system of differential equations for i, d, and a. Such a system will take into account the influence of the far field data and the rotation of the front due to refraction as well as the influence of the singularity. Here we only consider the effect of the latter.

The leading order velocity term is not constant in the vicinity of the node. Rather it has a radial dependence. As a result the normal velocity along the front changes, and this causes a rotation in the shock front. To measure this effect we define τ_i and τ_d,

$$\tau_i = \left.\frac{\partial \mathbf{V}\cdot\mathbf{n}}{\partial r}\right|_I, \qquad \tau_d = \left.\frac{\partial \mathbf{V}\cdot\mathbf{n}}{\partial r}\right|_D. \quad (13)$$

Here $\mathbf{n}$ is the unit normal to the front in the counterclockwise direction, and $\mathbf{V}$ is the velocity field of the approximate elementary wave. A positive value

TABLE I

THE STRENGTH OF THE SINGULARITY AT THE NODE DECREASES AS M APPROACHES UNITY

$M = R_m$	$M = 1/R_m$	min l_1	max $\tilde{l}_1$	min γ
1	1	1	1	∞
4/3	0.75	0.954	1.046	4×10^6
2	0.50	0.892	1.108	6×10^2
10	0.10	0.695	1.305	10
∞	0	0.500	1.500	4

for τ_i indicates a widening of the angle of incidence at I. We *assume* that the resulting rate of rotation of the front at I is equal to the rate of change of the angle of incidence,

$$\frac{\delta i}{\delta t} = \tau_i. \tag{14a}$$

A similar argument applies to τ_d and in particular

$$\frac{\delta d}{\delta t} = \tau_d. \tag{14b}$$

The rate of evolution of an approximate elementary wave depends on the magnitudes of τ_i and τ_d. However, these are essentially determined by the degree of singularity of V at the node. Hence, rapid evolution of the wave is most likely when $R_m \gg 1$. On the other hand when $R_m \approx 1$ then τ_i and $\tau_d \approx 0$ and the evolution of the wave is mainly controlled by the far field data.

To decide if an exact elementary wave is stable we consider all nearby approximate elementary waves and compute τ_i and τ_d for them. If the signs of τ_i and τ_d indicate an evolution toward the exact elementary wave then it is stable. Figures 8(a) and (b) show, respectively, the signs of τ_i and τ_d for

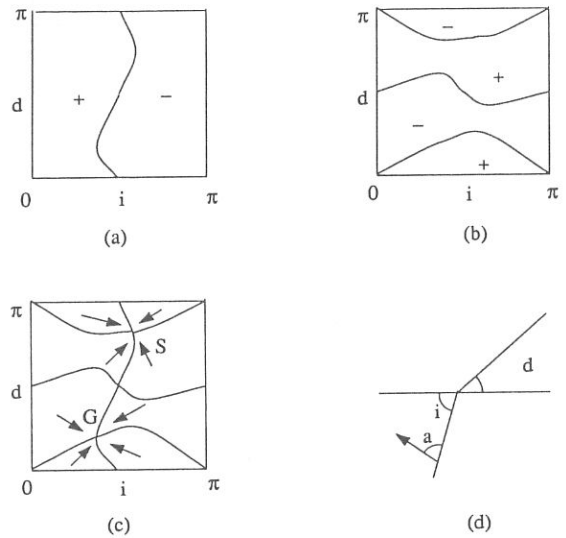

FIG. 8. (a) The sign of τ_i, gives the direction of change of i. (b) The sign of τ_d gives the direction of change of d. (c) Schematic diagram for the evolution of the front. (d) The flow is from Sectors 1 and 2 into 4 and 3. Here $M = 0.1$ and $R_k = 5$.

approximate elementary waves with $M = 0.1$ and $R_k = 5$. Figure 8(c) combines the results revealing that points G and S represent the only two stable solutions. G corresponds to a solution of (9) where $i_{hyp} = \alpha_1 = \pi - i$, $d_{hyp} = \alpha_3 = \pi - d$, and the flow is from the fast layer into the slow layer. (See Fig. 5(d).) This solution is called a G-wave. S corresponds to a second solution of (9) where $i_{hyp} = \alpha_2 = d$, $d_{hyp} = \alpha_4 = i$, and the flow is from the slow layer into the fast layer. (See Fig. 5(c).) This solution is called an S-wave.

From (13) it is immediately clear that a reversal of velocity changes the signs of τ_i and τ_d. Hence if an elementary wave is stable then under velocity reversal it becomes unstable. The velocity reversal also changes the mobility ratio from M to $1/M$. Therefore $M = 1$ is the critical mobility ratio. Numerical computations of τ_i and τ_d have consistently shown that (I) For $M < 1$ the points G and S represent stable solutions. (II) There are no stable elementary waves for $M > 1$. (III) The solutions on the curve Γ are not stable for $R_m \neq 1$.

The approximate solution described in Proposition 2 is also unstable. However, due to an extremely weak singularity, its relaxation time is typically much longer than the contact time between the layer and the advancing front. As a result the configuration of this wave persists for the duration of the contact.

6.3. *The Sensitivity of Stable Solutions*

For the G-wave, the incoming segment of the front is in the fast layer ($K > 1$), while for the S-wave the incoming portion of the front is in the slow layer ($K < 1$). As a result the G-wave and the S-wave have different sensitivities to perturbations. This fact, which is not reflected in (14), is caused by the asymmetrical role of i_{hyp} and d_{hyp} in determining the evolution of the front. In Fig. 7 we see that in the G-wave d_{hyp} is not sensitive to the angle of the incoming front i_{hyp}, since near G and for a fixed $a = 90°$, $|\delta d_{hyp}/\delta i_{hyp}| = |\delta d/\delta i| \ll 1$. However, the S-wave is very sensitive because near S we have $|\delta d_{hyp}/\delta i_{hyp}| = |\delta i/\delta d| \gg 1$. As a result it is more difficult to capture the S-wave than the G-wave. Moreover, the G-wave has a larger tolerance for i_{hyp} than d_{hyp}.

7. Numerical Experiments

To verify the results of the stability analysis we performed several numerical experiments. The numerical implementation is independent of our formal analysis and the two approaches give consistent conclusions. In particular we show the stability of the G-wave while the S-wave is shown to have a much weaker stability. The following four sections explain the numerical method for solving (1), the algorithm for the propagation of the node and refraction of the front, the experimental design, and the case studies.

7.1. *Front Tracking Method*

The numerical experiments reported here use the front tracking method [21–24]. In front tracking the wave front is introduced as a computational degree of freedom in the calculation. A dynamic grid generator aligns the mesh with the discontinuity curves and the propagation of the front is based directly on the dynamics of flow equations at the discontinuity. The direct use of one-dimensional Buckley–Leverett dynamics in the front propagation step gives optimal resolution for these waves.

Front tracking as applied to (1) consists of three steps—computation of the pressure, propagation of the discontinuity curves, and computation of the saturation. Given the initial and boundary conditions and the initial front we compute the pressure and velocity using a finite element method to solve (1b, 1c). The front is then propagated by using the theoretical solution of the associated Riemann problem. Finally we propagate the saturation in the interior regions (where the solution is smooth) by solving (1a) using, for example, the Engquist–Osher upstream weighting method [25].

7.2. *The Node Propagator Routine*

We propagate a front by moving a finite subset of its points along the direction normal to the front. However, near the node a special propagation

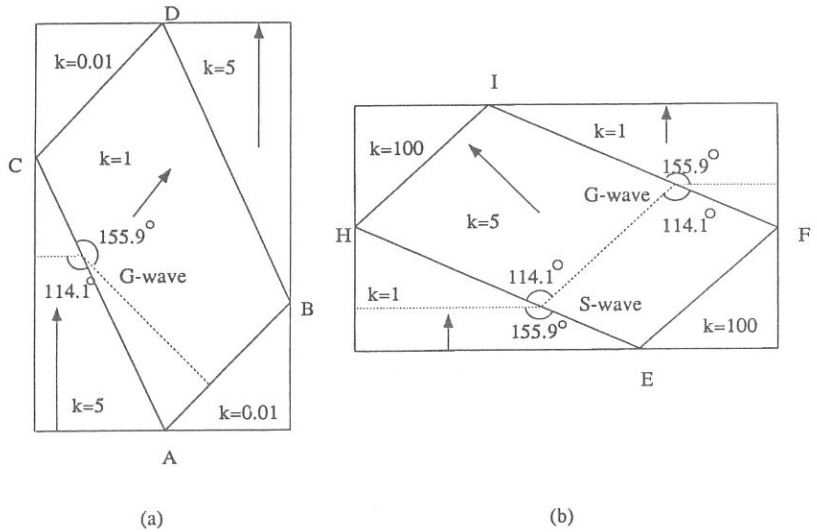

FIG. 9. The computational regions for testing the stability of G- and S-waves. The horizontal edges are Dirichlet boundaries and vertical edges are zero Neumann boundaries for the pressure field. The direction of the main flow and the value of the permeability $k(\mathbf{x})$ of each region are identified. The dashed lines represent the exact elementary waves for the given permeabilities (they meet the Neumann boundaries at 90°).

routine is needed to account for the two-dimensional character of the wave. Here we briefly describe our implementation which is based on the dynamical consistency condition, hyperbolic stability, and compatibility with known Riemann solutions (i.e., the $M = 1$ case).

We use the velocity field near the node to distinguish between the upstream and downstream sides. Then, by hyperbolic stability, the section of the front on the upstream side defines the true incident front. To propagate the front near the node at time t we first find the new node location for time $t + \Delta t$ by propagating the incident front and finding its intersection with the layer. (At this step we ignore the refraction of the front by the layer and if necessary we extrapolate the incident front to obtain the intersection.) Then we apply the dynamical consistency condition by setting the newly deflected section of the front at an angle that takes into account the velocity field of the deflected side.

7.3. *The Design of the Experiments*

The singularity at the node is the driving force for the evolution of approximate elementary waves and the formation of exact solutions. However, the singularity is weak and its effect can be dominated by the higher order terms in the eigenfunction expansion for the velocity. If the influence of the

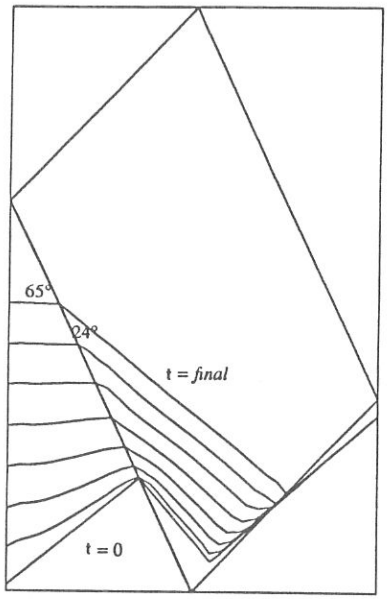

FIG. 10. A test of the stability of the G-wave where the mobility ratio is $M = 0.1$ and the permeability ratio is $R_k = 5$. The picture superimposes several steps in the evolution of the advancing shock front.

TABLE II
CONVERGENCE TO G-WAVE OCCURS WHEN $M \ll 1$ (HERE $R_k = 5$)

		Experiment					Theory
M	t	0.00	0.25	0.50	0.75	1.00	∞
0.10	i_{hyp}	146	123	119	117	115	114.1
0.10	d_{hyp}	96	160	159	157	156	155.9
0.50	i_{hyp}	146	137	130	125	119	114.1
0.50	d_{hyp}	96	162	161	160	160	155.9
0.75	i_{hyp}	146	142	139	136	130	114.1
0.75	d_{hyp}	96	163	163	162	162	155.9

far field velocities is not carefully controlled it is unlikely that the elementary waves will be observed on the grid sizes available to our study. Therefore the geometry and the boundary conditions for these experiments were designed to provide far field velocities consistent with the elementary wave solutions.

The experimental configurations are shown in Fig. 9. Both designs allow an elementary wave (the dotted line) to extend from the node out to a boundary. In Fig. 9(a) the two triangular regions at the lower right and upper left corners have very low permeabilities. These regions have a negligible flow and the layer interfaces AB and CD act approximately as Neumann boundaries, i.e., there is minimal flow across these curves. In Fig. 9(b) the two triangular regions at the lower right and the upper left have very high permeabilities and the layer interfaces EF and HI act approximately as Dirichlet boundaries, i.e., the flow direction is normal to these curves.

7.4. *Case Studies*

We performed two types of stability tests. In the first group of experiments we used the geometry of Fig. 9(a). Initially a shock front was located at

TABLE III
CONVERGENCE TO G-WAVE OCCURS WHEN $M \ll 1$ (HERE $R_k = 5$)

		Experiment					Theory
M	t	0.00	0.25	0.50	0.75	1.00	∞
0.10	i_{hyp}	74	105	111	114	115	114.1
0.10	d_{hyp}	165	148	150	152	156	155.9
0.50	i_{hyp}	74	87	93	98	102	114.1
0.50	d_{hyp}	165	148	147	149	151	155.9
0.75	i_{hyp}	74	86	84	90	96	114.1
0.75	d_{hyp}	165	151	149	149	150	155.9

TABLE IV
STABILITY OF G-WAVE TO PERTURBATIONS OF THE PERMEABILITY RATIO (HERE $M = 0.1$)

		Experiment					Theory
R_k	t	0.00	0.25	0.50	0.75	1.00	∞
5	i_{hyp}	128	121	119	117	114	114.1
5	d_{hyp}	83	139	147	156	155	155.9
3	i_{hyp}	128	120	120	120	120	120.0
3	d_{hyp}	100	149	150	150	150	150.0
15	i_{hyp}	128	113	110	107	104	104.5
15	d_{hyp}	100	168	168	168	167	165.5

arbitrary angles with respect to the layer AC. The subsequent evolution of the front was then used to study and validate the stability properties and the convergence rate for the elementary wave. In the second group of experiments we used Fig. 9(b) and varied the permeability of the central region. The local formation of the resulting elementary wave was then studied. Figures 11–14 show the results of these case studies. Each figure displays the superimposed positions of the front at certain time steps.

Figure 10 demonstrates the stability of the G-wave where $M = 0.1$ and $R_k = 5$. Two other experiments were conducted using the same configuration but with different values of M. The results are summarized in Table II. The rows of data in Table II list the node angles $i_{hyp}(t)$ and $d_{hyp}(t)$, in degrees, for the time development of the front. The column under "theory" shows the corresponding angles for the G-wave from (9). The first two rows of data correspond to Fig. 10. In this case the elementary wave formed rapidly. Lines

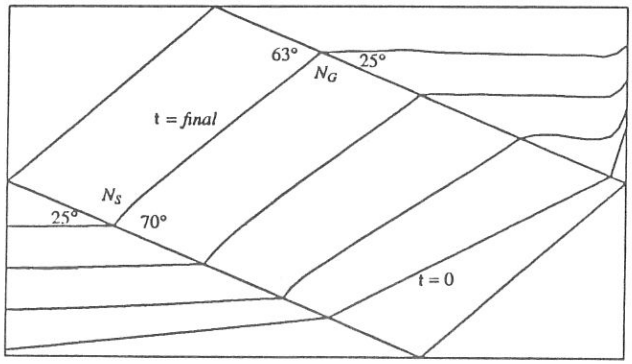

FIG. 11. An S-wave (at N_S) and a G-wave (at N_G) evolve from the interaction of the front and the layer. The S-wave is more sensitive to perturbations than the G-wave and evolves more erratically.

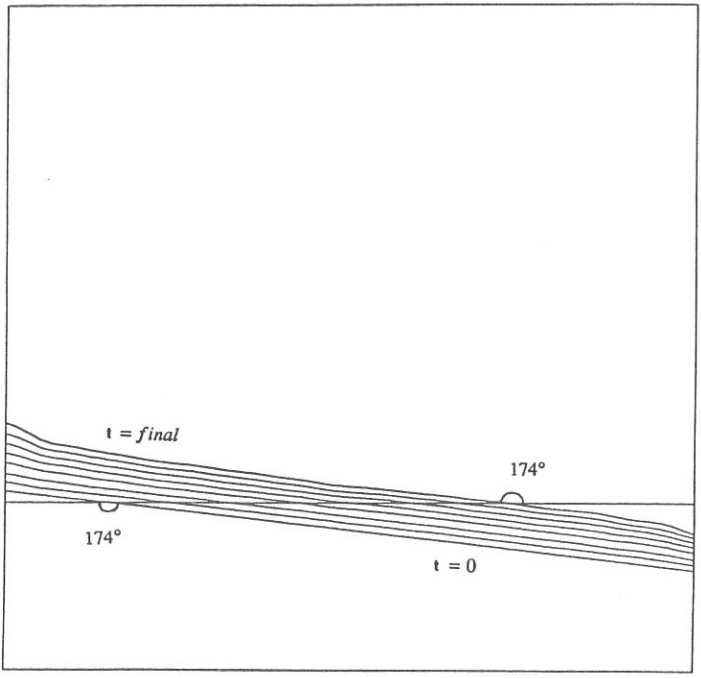

FIG. 12. A shock front crossing a layer at a small angle does not deflect. Here the flow is in vertical direction.

3 and 4 of Table II show a run with $M = 0.5$ and $R_k = 5$. We see that the final angles deviate from the theoretical values by about 5°. Lines 5 and 6 correspond to a run with $M = 0.75$ and $R_k = 5$. In this case the deviations from theoretical values, especially for i_{hyp}, are very large. Table III summarizes the results of three experiments similar to those in Table II but with a different initialization of the front position.

We see that the convergence of approximate waves to a G-wave is likely only if $M \ll 1$. For $M = 0.75$ the singularity is weak and the evolution toward the G-wave is no longer visible. In fact the final angles in the latter case agree with the unit mobility ratio case (7), rather than (9), to within 2°. Therefore $0.75 \leqslant M \leqslant 1$ can only support a passive refraction and in this case one can use (7) to estimate d accurately. These results are in general agreement with the stability analysis and the estimate for the strength of the singularity.

Now we use the setup shown in Fig. 9(b) to study the stability of the G-wave to perturbations of the permeability ratio, while the mobility ratio is fixed at $M = 0.1$. In these experiments the far field velocities are not identical with the velocity field of the forming elementary waves. Hence the results give a stronger confirmation of the stability of the G-waves. In Table IV the

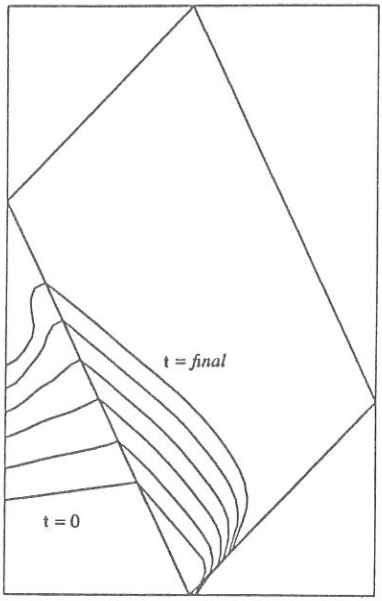

FIG. 13. An experiment similar to that in Fig. 10 except the mobility ratio is larger than 1, $M = 5$. A slight perturbation of the front leads to the formation of a narrow finger.

first two rows of data correspond to the angles at the upper node N_G in Fig. 11, where the permeability of the central region is 5. In lines 3 and 4, we show the results for changing the permeability of the central region from 5 to 3. We expect the time-asymptotic front to have $i_{hyp} = 120°$ and $d_{hyp} = 150°$. This means that, compared to Fig. 11, the time-asymptotic front will bend backward by about 6° at N_G. In lines 5 and 6 we repeat the above experiment for a central region permeability of 15. Now we expect the time-asymptotic front to have $i_{hyp} = 104.5°$ and $d_{hyp} = 165.5°$. Thus, compared to Fig. 11, the front will bend forward by about 10° at N_G. In these experiments the time development of the G-wave confirmed the theoretical predictions.

Figure 11 also shows the evolution of the S-wave (at the lower node N_S). The value of d_{hyp} at the final time step differs by 4° from the theoretical value. In other experiments, with a different initialization of the front, we observed an erratic transition toward the S-wave. This wave is more sensitive to perturbations than the G-wave, since its upstream side corresponds to the slower layer. In particular d_{hyp} may oscillate around the theoretical value.

Figure 12 shows a shock front crossing a horizontal layer at a small angle. We see that the front is not deflected, in agreement with the prediction of Proposition 2. This result is independent of the permeability and mobility ratios but it is necessary that the velocity direction near the node should not make a small angle with the layer.

Figure 13 shows the result of an experiment similar to Fig. 10 but with the mobility ratio $M = 5$. For $M > 1$ the exact elementary wave is not stable and we see the common occurrence of a finger originating at the node.

Figure 14 shows a shock front interacting with a vertical layer interface. Here the mobility ratio is $M = 10$ and the permeability of the left layer is 5 times the permeability of the right layer. It appears that the time-asymptotic front and the flow direction become tangential to the layer at the node. Our numerical results in this case, especially the appearance of the finger, qualitatively agree with the experimental and computational results of Orr and coworkers [26].

8. Conclusions

Using formal and numerical methods, a consistent analysis of wave refraction in two-phase incompressible flow has been performed. Stability of elementary wave solutions has been determined. Within the formal framework of this paper, the uniform asymptotics of scale invariance symmetry breaking

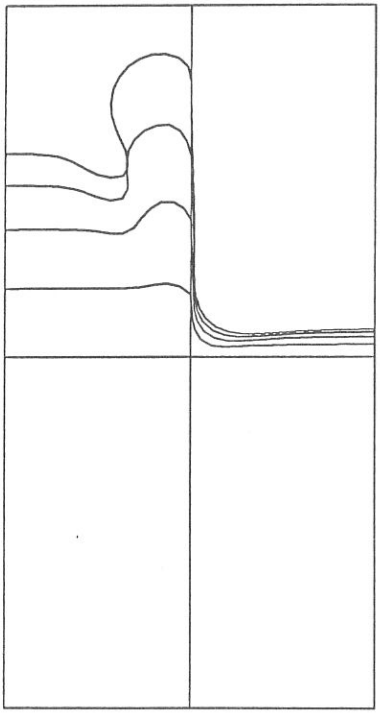

FIG. 14. The interaction of a shock front and a vertical layer. Here $M = 10$ and the permeability of the left side is 5 times the permeability of the right side. The flow is in vertical direction.

is developed, and the need for scale symmetry breaking approximate elementary waves is indicated.

9. Acknowledgments

This paper is an edited version of a doctoral dissertation submitted in partial fulfillment of the requirements for the degree of Doctor of Philosophy in the Courant Institute of Mathematical Sciences at the New York University. This dissertation was written under the direction of Professor James Glimm, to whom I am deeply grateful for inspiration and guidance. I also thank Professor Brent Lindquist for supervising numerical implementations and experiments.

References

1. A. Tveito and R. Winther, *Existence, Uniqueness and Continuous Dependence for a System of Hyperbolic Conservation Laws Modelling Polymer Flooding,* preprint, Institutt for Informatikk, Universitetet i Oslo (1990).
2. E. L. Isaacson, D. Marchesin, B. Plohr, and B. Temple, The Riemann problem near a hyperbolic singularity: The classification of solutions of quadratic Riemann problems, I, *SIAM J. Appl. Math.* **48,** no. 5, 1009–1032 (1988).
3. E. L. Isaacson and B. Temple, The Riemann problem near a hyperbolic singularity, II, *SIAM J. Appl. Math.* **48,** no. 6, 1287–1301 (1988).
4. E. L. Isaacson and B. Temple, The Riemann problem near a hyperbolic singularity, III, *SIAM J. Appl. Math.* **48,** no. 6, 1302–1318 (1988).
5. D. G. Schaeffer and M. Shearer, "The classification of 2×2 systems of non-strictly hyperbolic conservation law, with application to oil recovery," *Comm. Pure Appl. Math* **40,** 141–178 (1987).
6. W. Fickett and W. C. Davis, *Detonation,* Univ. of California Press, Berkeley, 1979.
7. J. J. Erpenbeck, Stability of idealized one-reaction detonations, *Phys. Fluids.* **7,** 684–696 (1964).
8. A. Majda and R. Rosales, A theory for spontaneous Mach stem formation in reacting shock fronts. I. The basic perturbation analysis, *SIAM J. Appl. Math.* **43,** 1310–1334 (1983).
9. A. Majda and R. Rosales, A theory for spontaneous Mach stem formation in reacting shock fronts. II. Steady wave bifurcations and the evidence for breakdown, *Stud. Appl. Math.* **71,** 117–148 (1984).
10. J. Glimm and D. H. Sharp, Elementary waves for hyperbolic equations in higher dimensions: An example from petroleum reservoir modeling, *Contemp. Mathem.* **60,** 35–41 (1987).
11. P. Lax, *Hyperbolic Systems of Conservation Laws and the Mathematical Theory of Shock Waves,* SIAM, Philadelphia (1973).
12. O. A. Oleinik, Uniqueness and stability of the generalized solution of the Cauchy problem for a quasi-linear equation, English Trans., *Amer. Math. Soc. Transl. Ser. 2* **33,** 285–290 (1963).
13. S. N. Kruzkov, First order quasilinear equations in several independent variables, *Math. USSR-Sb.* **10,** 217–243 (1970).
14. E. Isaacson, D. Marchesin, and B. Plohr, Transitional waves for conservation laws, *SIAM J. Math. Anal.,* to appear.

15. H. P. Langtangen, A. Tveito, and R. Winther, *Instability of Buckley–Leverett Flow in Heterogeneous Media,* preprint, Institutt for Informatikk, Universitetet i Oslo (1990).
16. J. Glimm, Elementary waves and Riemann solutions: Their theory and their role in science." *In Proceedings of Seminar on Differential Equations, Hsinchu, Taiwan, June 3–7, 1985,* pp. 65–74.
17. D. Wagner, The Riemann problem in two space dimensions for a single conservation law, *Math. Ann.* **14,** 534–559 (1983).
18. J. Guckenheimer, Shocks and rarefactions in two space dimensions, *Arch. Rational Mech. Anal.* **59,** 281–291 (1975).
19. B. Lindquist, Construction of solutions for two dimensional Riemann problems, *Adv. Hyperbolic Partial Differential Equations Comput. Math. Appl.* **12A,** 615–630 (1986).
20. M. Maesumi, *Approximate Scale Breaking Nonlinear Elementary Waves for Two Phase Incompressible Flow in Porous Layered Media,* Thesis, Courant Institute, New York University (1990).
21. J. Glimm, Tracking of interfaces in fluid flow: Accurate methods for piecewise smooth problems, transonic shock and multidimensional flows. *In* Richard E. Meyer (Ed.), *Advances in Scientific Computing,* Academic Press, New York (1982).
22. J. Glimm, B. Lindquist, O. McBryan, and L. Padmanhaban, A front tracking reservoir simulator: 5-spot validation studies and the water coning problem. *Frontiers in Applied Mathematics,* Vol. 1, SIAM, Philadelphia (1983).
23. J. Glimm, E. Isaacson, D. Marchesin, and O. McBryan, Front tracking for hyperbolic systems, *Adv. in Appl. Math.* **2,** 91–119 (1981).
24. O. McBryan, Elliptic and hyperbolic interface refinement. *In* J. Miller (Ed.), *Boundary Layers and Interior Layers—Computational and Asymptotic Methods,* Boole Press, Dublin (1980).
25. Engquist and Osher, Stable and entropy satisfying approximations for transonic flow calculations, *Math. Comp.* (1980) **34,** 45–75.
26. D. C. Brock, F. M. Orr, and H. A. I. M. Tchelepi, *Viscous Fingering and Gravity Segregation During Miscible Displacement in Heterogeneous Porous Media.* Presented at the 11th International Workshop and Symposium on Enhanced Oil Recovery, sponsored by the international Energy Agency and the Institut Français du Petrole, Rueil-Malmaison, France (October 8–10, 1990).